1 Introduction to Cone Beam Computed Tomography

Shawneen M. Gonzalez

Introduction

This chapter covers basics of cone beam computed tomography including comparison to traditional computed tomography, artifacts frequently seen, and views created with a cone beam computed tomography dataset.

Conventional Computed Tomography

General Information

Computed tomography (CT) is credited to Godfrey Hounsfield, who in 1967 wrote about the technology and then created a unit in 1972. He was awarded the Nobel Prize in Physiology/Medicine in 1979. Conventional CT units are both hard-tissue and soft-tissue imaging modalities. The first CT, first generation, had a scan time of 10+ minutes depending on how much of the body was being imaged. The processing time would take 2½ hours or longer. All first-generation CT units were only a single slice. This means that one fan of radiation exposed the patient and would have to circle around the patient several times to cover the area of concern. Current CT units are fifth generation, or helical/spiral. The scan times have gone down to 20–60 seconds with a processing time of 2–20 minutes. The number of slices available is up to 64, 128, 256, and 512+. The more slices available makes it possible to scan more of the patient in one circle, hence the shorter scan times. Conventional CT units work with the patient lying down on a table while being scanned. The table moves in and out of the bore to cover the area of concern. Once all the data are received,

Interpretation Basics of Cone Beam Computed Tomography, Second Edition.
Edited by Shawneen M. Gonzalez.

Companion website: www.wiley.com/go/gonzalez/interpretation

they are compiled to create a dataset. This dataset can be manipulated to look at the information in many different angles.

Cone Beam Computed Tomography

General Information

Cone beam computed tomography (CBCT) was developed in Italy in 1997. The first unit created was the NewTom. The NewTom was similar to conventional CT in having the patient lying down with an open bore where the radiation exposes the patient. Instead of a fan of radiation (used in conventional CT units), a cone of radiation is used to expose the patient, hence the name cone beam computed tomography. As new CBCT units were created, companies started using seated or standing options. With continued updates to the units, the sizes have become smaller, with many needing only as much space as a pantomograph machine.

Conventional CT versus Cone Beam CT

Voxels

Voxels are 3D data blocks representing a specific x-ray absorption. CBCT units capture isotropic voxels. An isotropic voxel is equal in all three dimensions (x, y, and z planes), producing higher-resolution images compared to conventional CT units. Conventional CT unit voxels are non-isotropic with two sides equal, but the third side (z-plane) different. The voxel sizes currently available in CBCT units range from 0.076 mm to 0.6 mm. The voxel sizes currently available in conventional CT units range from 1.25 mm to 5.0 mm. Resolution of the final image is determined by the unit's voxel size. The smaller the voxel size the higher the resolution.

Field of View

Field of view (FOV) is the area of the patient captured. CBCT units vary in FOV options, with some units having a fixed FOV and some having variable FOVs. The ranges of FOVs are from 5 cm × 3.8 cm, commonly referred to as a small/quadrant FOV, to 23 cm × 26 cm, commonly referred to as a large FOV (Figures 1.1–1.6).

Radiation Doses

Radiation doses with CBCT units are as varied as the FOV options. CBCT units have approximate radiation dose ranges of 5 microSieverts to 1073 microSieverts. Conventional CT units have much higher radiation doses due to their soft tissue capabilities, with doses of 1200 microSieverts and higher per each scan, depending on the selected scan field.

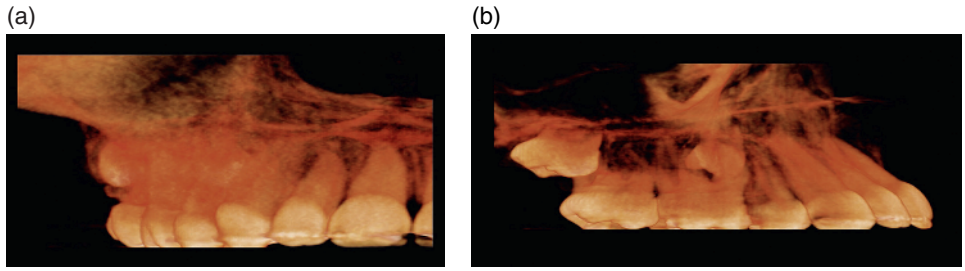

Figure 1.1. (a) 3D rendering of a small FOV of 5 cm × 8 cm from an anteroposterior (AP) view. (b) 3D rendering of a small FOV of 5 cm × 8 cm from a lateral view.

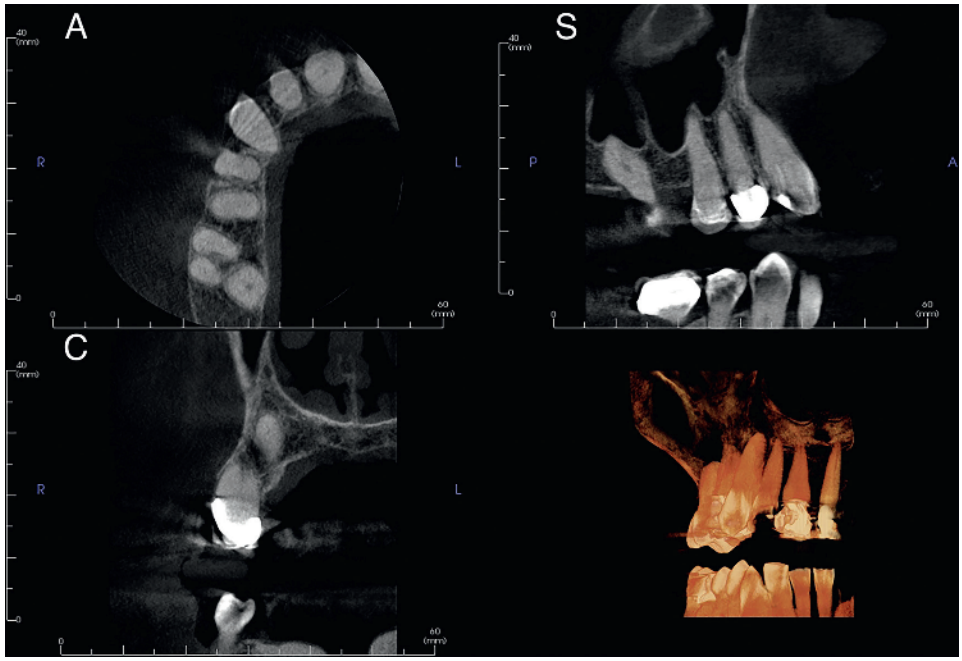

Figure 1.2. Axial (A), coronal (C), sagittal (S), and reconstructed 3D views from a small FOV.

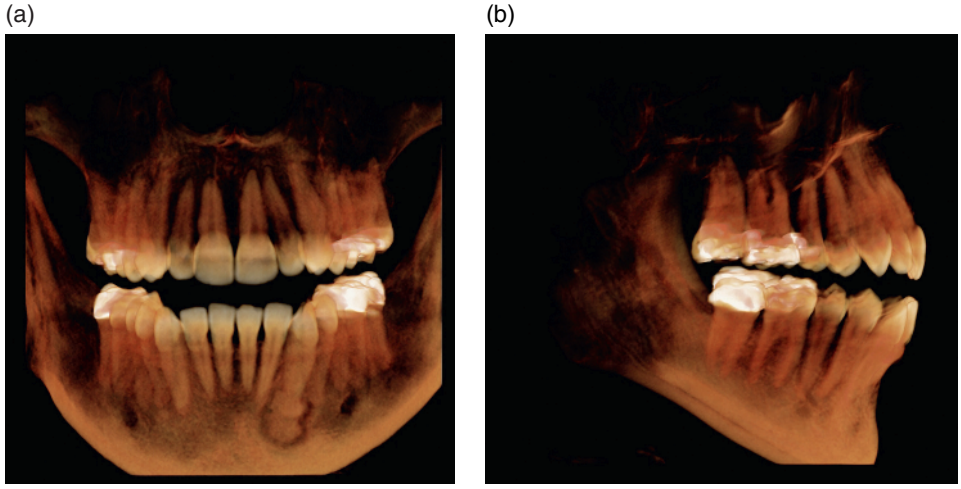

Figure 1.3. (a) 3D rendering of a medium FOV of 8 cm × 8 cm from an anteroposterior (AP) view. (b) 3D rendering of a medium FOV of 8 cm × 8 cm from a lateral view.

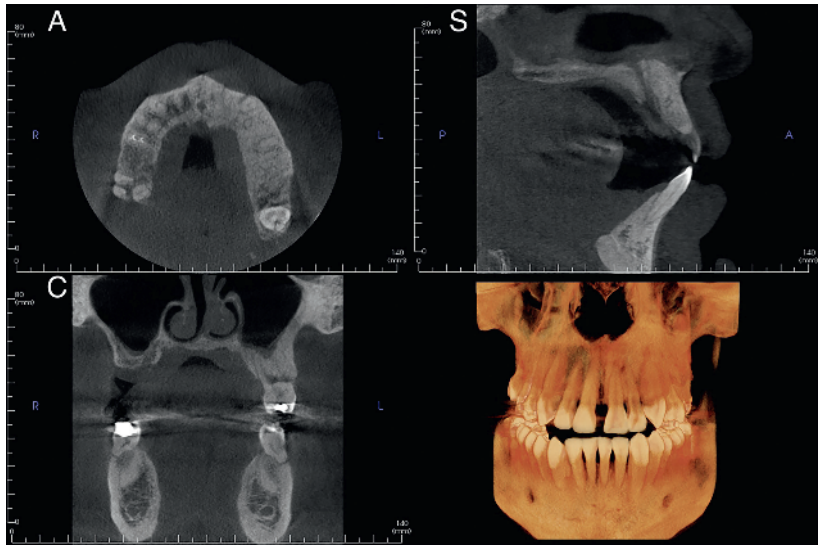

Figure 1.4. Axial (A), coronal (C), sagittal (S), and reconstructed 3D views from medium FOV.

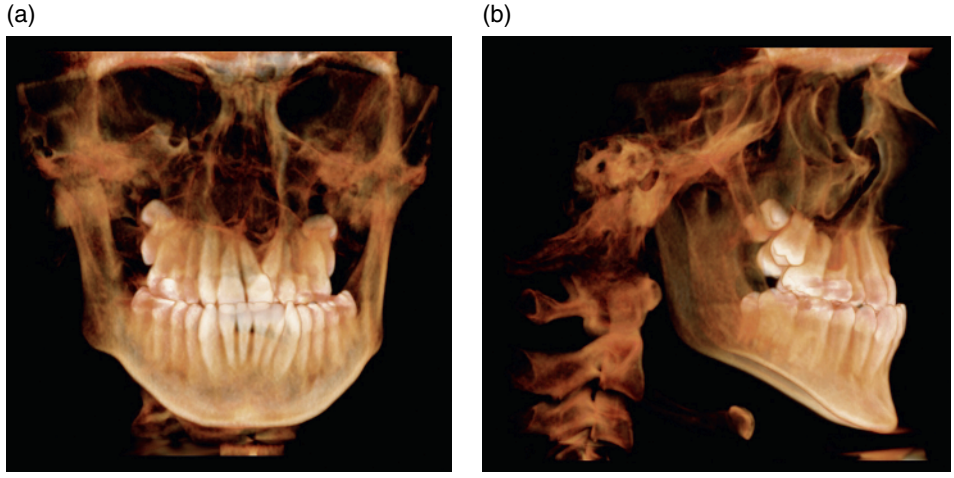

Figure 1.5. (a) 3D rendering of a large FOV of 16 cm × 16 cm from an anteroposterior (AP) view. (b) 3D rendering of a large FOV of 16 cm × 16 cm from a lateral view.

Viewing CBCT Data

Multiplanar Reformation

Multiplanar reformation, or MPR, is a view of three different directional 2D images (axial, coronal, and sagittal planes) (Figure 1.7). Within this view, the images may be manipulated in the thickness of data, and direction of viewing can be altered. Reconstructed pantomographs and lateral cephalometric skulls (Figures 1.8 and 1.9) are possible without distortion from standard 2D radiography. The dataset may also be manipulated to create cross-sectional (orthogonal) views of the jaws and condyles (Figures 1.10 and 1.11).

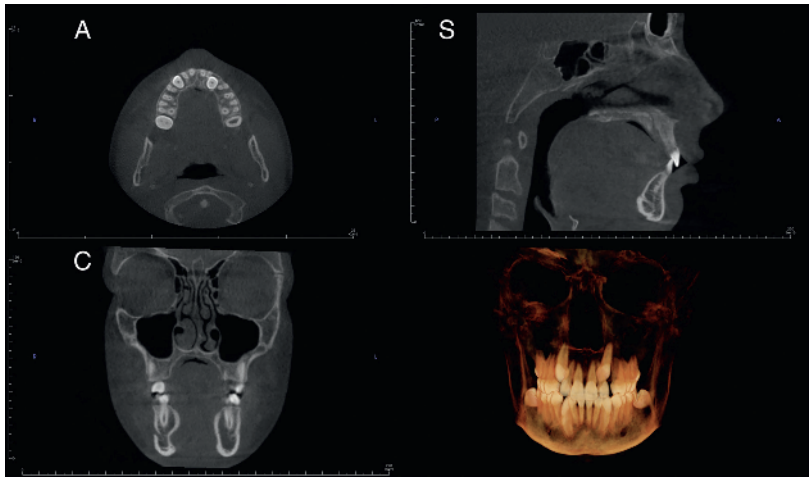

Figure 1.6. Axial (A), coronal (C), sagittal (S), and reconstructed 3D views from large FOV.

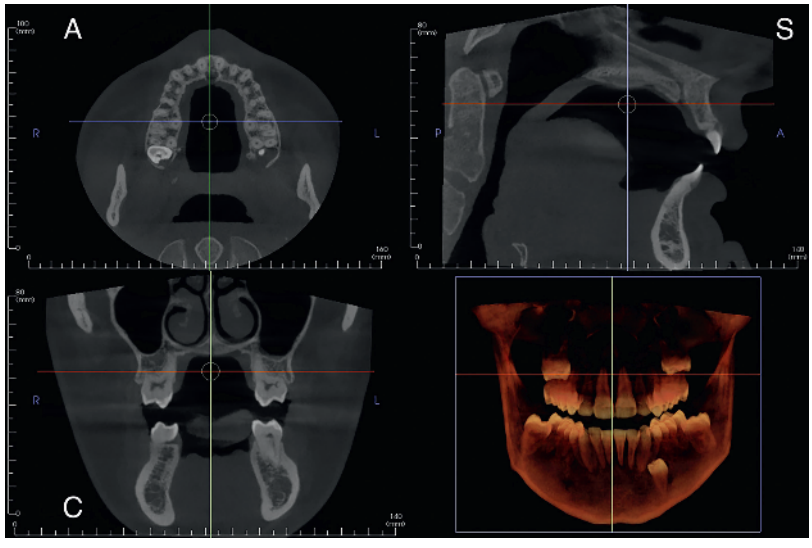

Figure 1.7. Axial (A), coronal (C), sagittal (S), and reconstructed 3D views.

Figure 1.8. Reconstructed pantomograph from a CBCT scan.

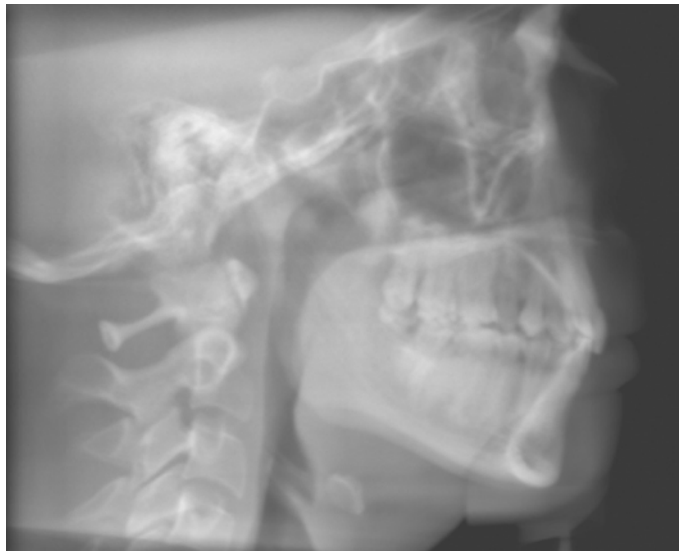

Figure 1.9. Reconstructed lateral cephalometric skull.

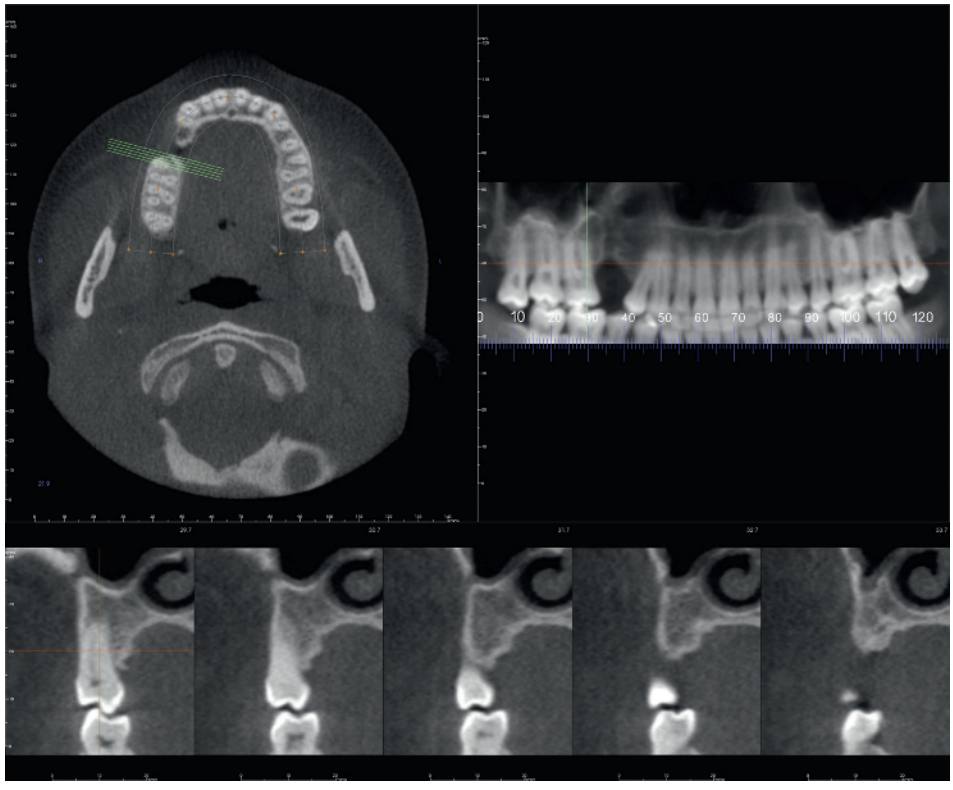

Figure 1.10. Cross-sectional slices with axial view and reconstructed pantomograph.

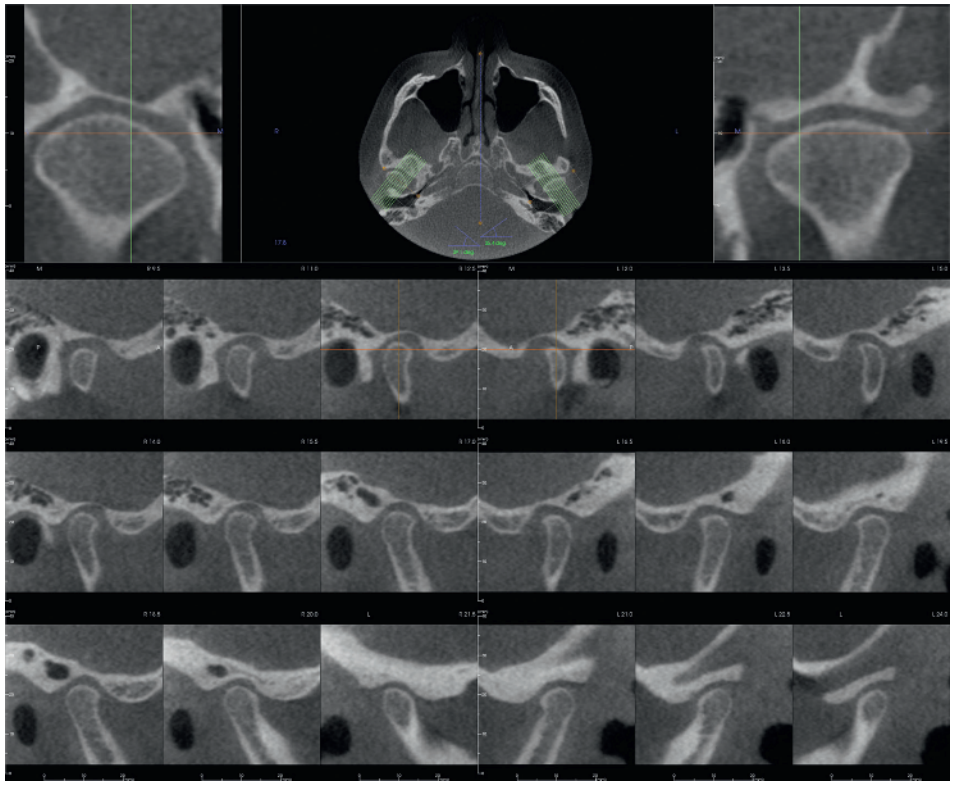

Figure 1.11. Temporomandibular joint view with rotated sagittal cross-sectional slices.

3D Rendering

The most common form of 3D rendering offered in CBCT software is indirect volume rendering, which determines the grays of the voxels to create a 3D image (Figure 1.12). Another form of 3D rendering is referred to as direct volume rendering, where the highest attenuation value for each voxel is used creating a maximum intensity projection (MIP) (Figure 1.13).

Artifacts

Streak Artifacts/Undersampling

Streak artifacts occur when an object with high density (such as metallic restorations) creates areas of undersampling where no viable information is recorded. These present as white streaks (Figure 1.14) radiating from the high-density object. Beam hardening artifact is caused when low energy x-rays are absorbed by high-density objects creating an increase in x-ray beam energy, which "hardens" the beam. This results as increased density (black) lines radiating from the high-density object (Figure 1.14). Care should be taken not to interpret anything in the streak artifacts

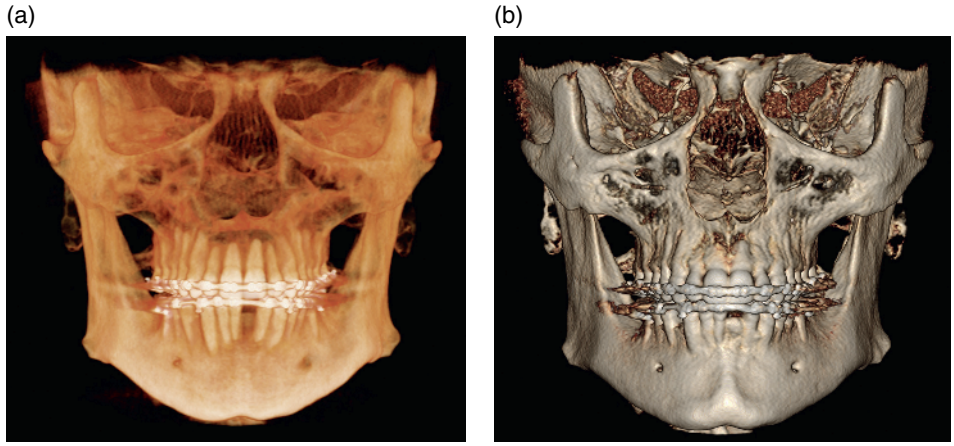

Figure 1.12. (a) 3D rendered view with teeth setting. (b) 3D rendered view with bone setting.

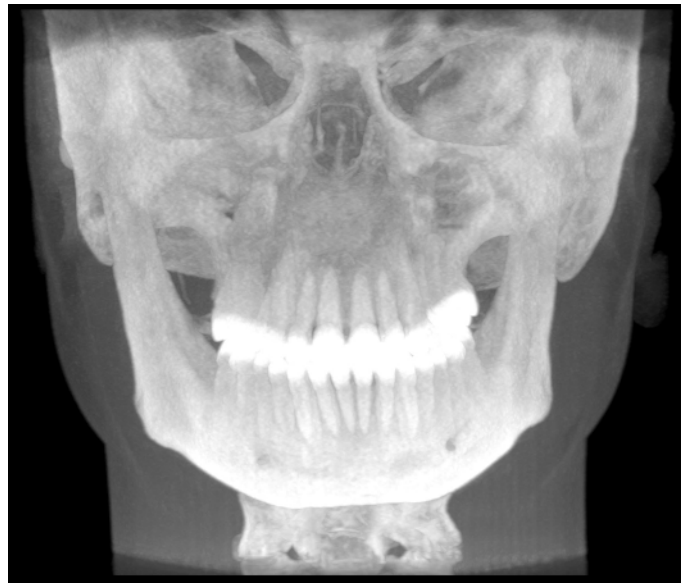

Figure 1.13. Maximum Intensity Projection (MIP) view.

and beam hardening. Aliasing is another form of undersampling, when too few images are acquired and appear as small lines throughout a scan (Figure 1.15).

Motion Artifacts

Motion artifacts occur due to either normal pathophysiological movement or when the patient moves during a scan. This presents as double bony borders to ill-defined bony borders (Figures 1.16 and 1.17). This can be minimized by restraining the patient's head and using as short a scan time as possible.

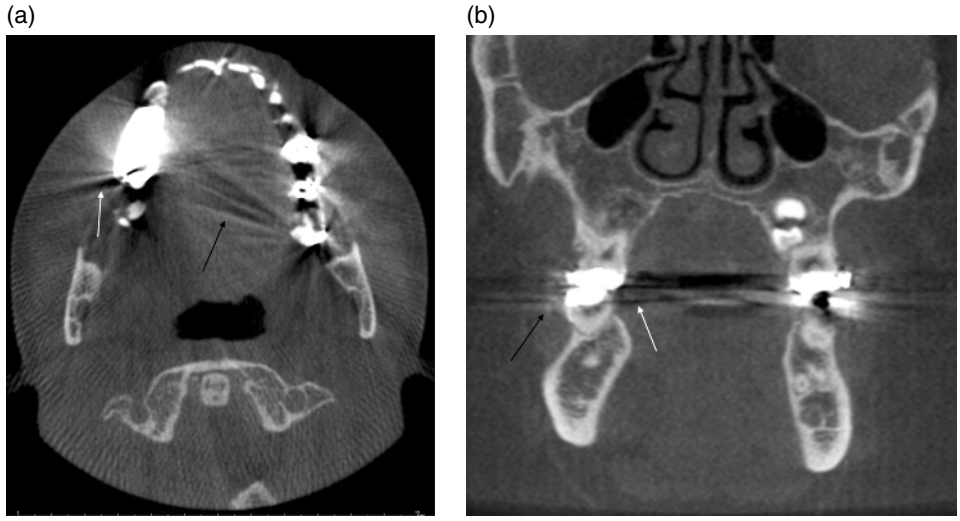

Figure 1.14. (a) Axial view showing streak artifact (black arrow) and beam hardening (white arrow) due to metallic restorations. (b) Coronal view showing streak artifact (black arrow) and beam hardening (white arrow) due to metallic restorations.

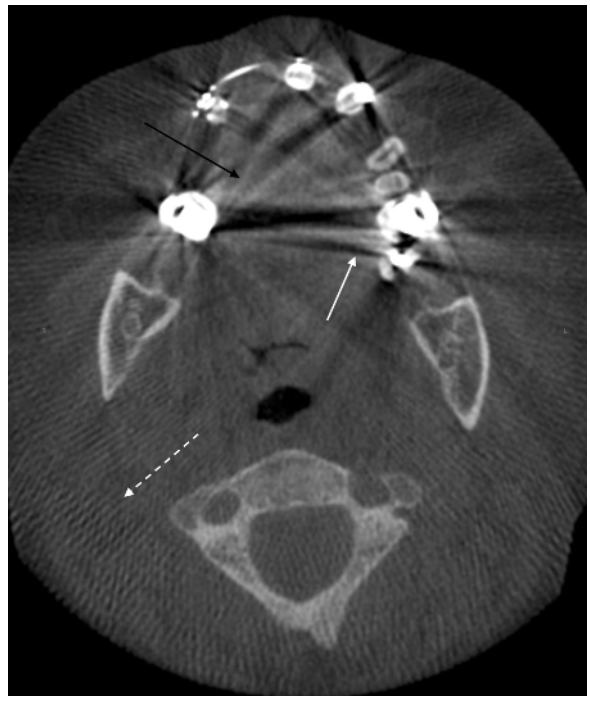

Figure 1.15. Axial view with metallic streak artifact (black arrow), beam hardening (white arrow), and aliasing of scan as linear radiolucent lines (white dotted arrow) throughout the entire image.

Ring Artifacts

Ring artifacts present as white or black circular artifacts. They typically indicate poor calibrations and imperfections in the scanner detection (Figure 1.18).

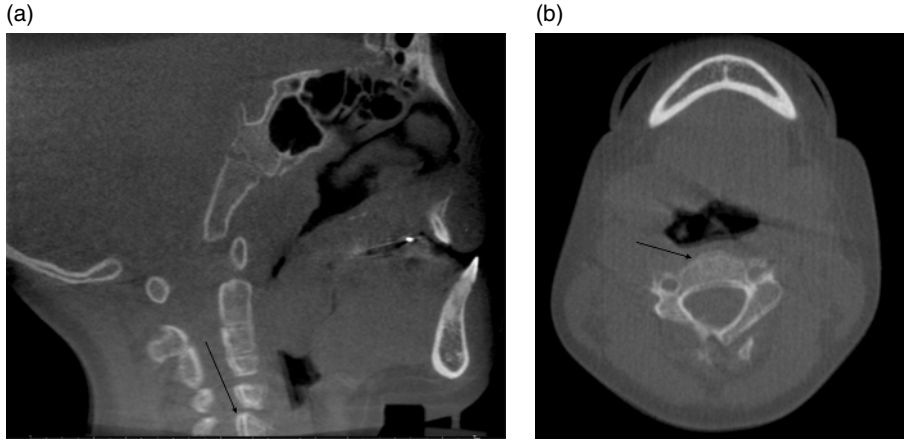

Figure 1.16. (a) Sagittal view showing motion artifact of the cervical vertebrae (black arrow). (b) Axial view showing motion artifact of the cervical vertebrae (black arrow).

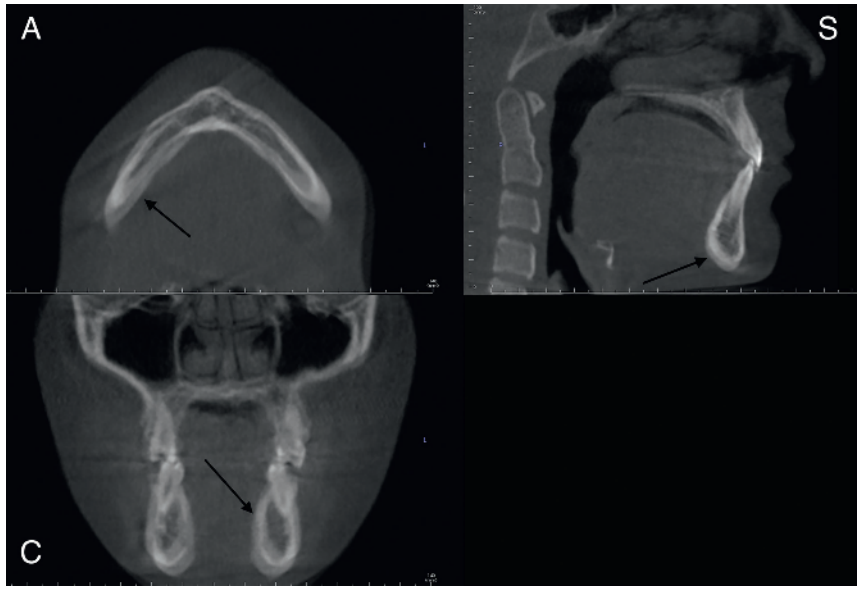

Figure 1.17. Axial (A), coronal (C), and sagittal (S) views with motion artifact (black arrows) throughout the jaws.

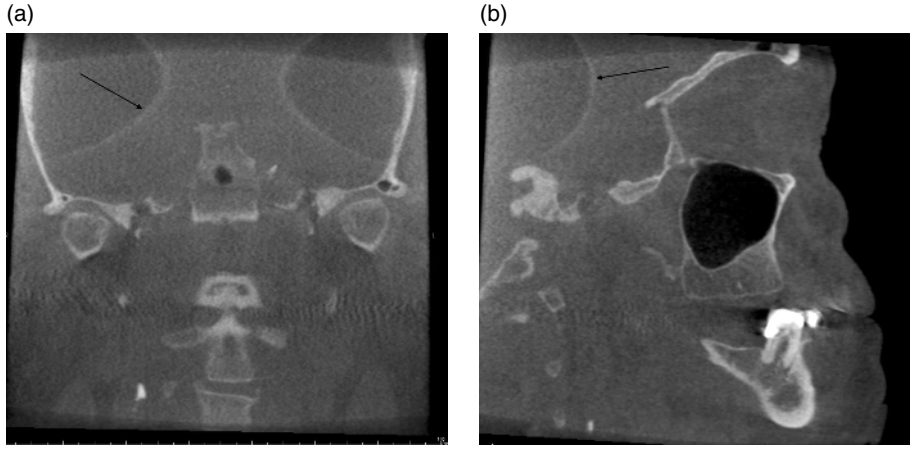

Figure 1.18. (a) Coronal view showing white ring artifacts (black arrow). (b) Sagittal view showing white ring artifacts (black arrow).

References

Conventional Computed Tomography and Cone Beam Computed Tomography

Dalrymple, N. C., Prasad, S. R., El-Merhi, F. M., et al. (2007). Price of isotropy in multidetector CT. *RadioGraphics*, **27**, 49–62.

Hounsfield, G. (1973). Computerized transverse axial scanning (tomography). 1. Description of the system. *Br J Radiol*, **46**, 1016–22.

Mallaya, S., and Lam, E. (Ed.). (2019). *White and Pharaoh's Oral Radiology: Principles and Interpretation*. Mosby.

Miles, D. E. (2008). *Color Atlas of Cone Beam Volumetric Imaging for Dental Applications*. Quintessence.

Popat, H., Drage, N., Durning, P. (2008). Mid-line clefts of the cervical vertebrae—an incidental finding arising from cone beam computed tomography of the dental patient. *Br Dental J*, **204**, 303–6.

Viewing CBCT Data

Cody, D. D. (2002). AAPM/RSNA physics tutorial for residents: topics in CT. *Image processing in CT. Radiographics*, **22**, 1255–68.

Mallaya, S., and Lam, E. (Ed.). (2019). *White and Pharaoh's Oral Radiology: Principles and Interpretation*. Mosby.

Artifacts

Mallaya, S., and Lam, E. (Ed.). (2019). *White and Pharaoh's Oral Radiology: Principles and Interpretation*. Mosby.

Pauwels, R., Araki, K., Siewerdsen, J. H., et. al. (2015). Technical aspects of dental CBCT: state of the art. *Dentomaxillofac Radiol*, **44**, 20140224.

Popilock, R., Sandrasagaren, K., Harris, L., et al. (2008). CT artifact recognition for the nuclear technologist. *J Nucl Med Technol*, **36**, 79–81.

Zoller, J. E., and Nuegebauer, J. (2008). *Cone-Beam Volumetric Imaging in Dental, Oral, and Maxillofacial Medicine*. Quintessence, Germany.